Sādhanā, Vol. 23, Parts 5 & 6, Oct & Dec 1998, pp. 459–480. © Indian Academy of Sciences

Behaviour analysis of numerical solutions and simulation of coherent structures in compressible mixing layers

FU DEXUN and MA YANWEN

LNM, Institute of Mechanics, CAS, Beijing 100 080, China
e-mail: fud@cc5.imech.ac.cn

Abstract. For understanding the correctness of simulations the behaviour of numerical solutions is analysed. In order to improve the accuracy of solutions three methods are presented. The method with GVC (group velocity control) is used to simulate coherent structures in compressible mixing layers. The effect of initial conditions for the mixing layer with convective Mach number 0.8 on coherent structures is discussed. For the given initial conditions two types of coherent structures in the mixing layer are obtained.

Keywords. Group velocity control; coherent structures; behaviour analysis of numerical solutions; compressible mixing layers.

1. Introduction

Numerical characteristics of simulated unsteady flow fields remain largely unclear as yet, and have to be studied for correct simulation of this kind of flows, such as turbulent flows.

For simulating complex flow fields, high-order accuracy schemes are needed in order to capture the flow field structures in a wide range of scales. When low-order accuracy schemes are used to simulate the turbulent flow, incorrect coherent structures with wrong dissipation and dispersion can be obtained. Many high-order accurate schemes have been developed (Rai & Moin 1991; Lele 1992; Fu Dexun & Ma Yanwen 1995; Ma Yanwen & Fu Dexun 1996).

The commonly used method to analyse the accuracy of schemes was assessed based on evaluation of dissipative error, but for unsteady flows, in addition to the dissipative error, influence of the group velocity of wave packets (or phase velocity) and harmonic content in numerical solutions are also important.

In the present paper, the behaviour of numerical solutions is analysed. For improving the resolution efficiency of the schemes, three methods are presented. They are: (1) Increasing the accuracy of approximation (IAA), (2) accuracy balance control (ABC), and (3) group velocity control (GVC). The GVC method is used to simulate the coherent structures in the compressible mixing layer. The effect of the initial conditions of the compressible mixing layer on coherent structures is discussed.

2. Behaviour analysis of numerical solutions

2.1 *Model equation*

Consider the following model equation and its semi-discrete approximation:

$$\frac{\partial u}{\partial t}+\frac{\partial f}{\partial x}=\frac{\partial}{\partial x}\mu\frac{\partial u}{\partial x};\ f=cu,\ c;\ \mu=\text{const.} \tag{1}$$

$$\frac{\partial u_j}{\partial t}+c\frac{F_j}{\Delta x}=\mu\frac{S_j}{\Delta x^2},\ -\infty<x<+\infty, \tag{2}$$

where $F_j/\Delta x$ is an approximation for $\partial u/\partial x$, $S_j/\Delta x$ is an approximation for $\partial^2 u/\partial x^2$. With initial condition $u(x,0)=\exp(ikx)$ the exact solution of (1) is as follows

$$u(x,t)=\exp(-\mu k^2 t)\exp[ik(x-ct)]. \tag{3}$$

With initial condition $u(x_j,0)=\exp(ikx_j)$ the exact solution for (2) can be written as

$$u(x_j,t)=\exp\left[-\mu k^2\frac{K_d}{(k\Delta x)^2}t-\frac{cK_r}{\Delta x}t\right]\exp\left[ik\left(x_j-c\frac{K_i}{k\Delta x}t\right)\right], \tag{4}$$

where $K_e=K_r+iK_i$ is the modified wave number and $\alpha=k\Delta x$. Comparing (4) with (3) it can be seen that K_i is related to the phase speed in numerical solutions, K_r is related to damping of the difference solution due to discretization of the convection term, K_d is related to physical dissipativity of the solution. For particular schemes analytical expressions for K_i, K_r and K_d can be obtained for the linear case. They are functions of $k\Delta x$. From (3) with $\mu=0$, it can be seen that all waves with different k have the same phase speed and uniform group velocity of wave packets. This means that the initial waves given at $t=0$ will keep the shape as time advances. But K_i, K_r and K_d are functions of $\alpha=k\Delta x$ in numerical solutions. This means that the error in numerical solutions of the schemes is different for different wave numbers k. Nonlinear dependence of K_i on α leads to nonuniform group velocity which is defined as $\mathrm{d}K_i/\mathrm{d}\alpha$ in the present paper. This is the reason for the production of the oscillations and the deviation of the moving direction of the wave packets with different wave numbers k in the numerical solutions (Trefethen 1982; Fu Dexun & Ma Yanwen 1997). From figure 1, it can be seen that different discretization can give good resolution for the lower wave numbers with $K_i/\alpha\sim 1$, $\mathrm{d}K_i/\mathrm{d}\alpha\sim 1$ and $K_r/\Delta x\sim 0$. The range of wave numbers k with correct simulation can be enlarged for higher order accurate schemes.

For semi-discrete approximation (2) after Taylor series expansion, we can get the corresponding modified equation

$$\frac{\partial u}{\partial t}+\frac{\partial f}{\partial x}=\frac{\partial}{\partial x}\left(\mu\frac{\partial u}{\partial x}\right)+\frac{\partial}{\partial x}\left(\mu'\frac{\partial u}{\partial x}\right)+\frac{\partial}{\partial x}\left(\mu_2\frac{\partial u}{\partial x}\right)+\frac{\partial}{\partial x}\left(a\frac{\partial^2 u}{\partial x^2}\right), \tag{5}$$

where

$$\mu'=\left[\sum\mu'_{2m}\Delta x^{2m-2}\frac{\partial^{2m-1}u}{\partial x^{2m-1}}\right]\Big/\frac{\partial u}{\partial x}, \tag{6a}$$

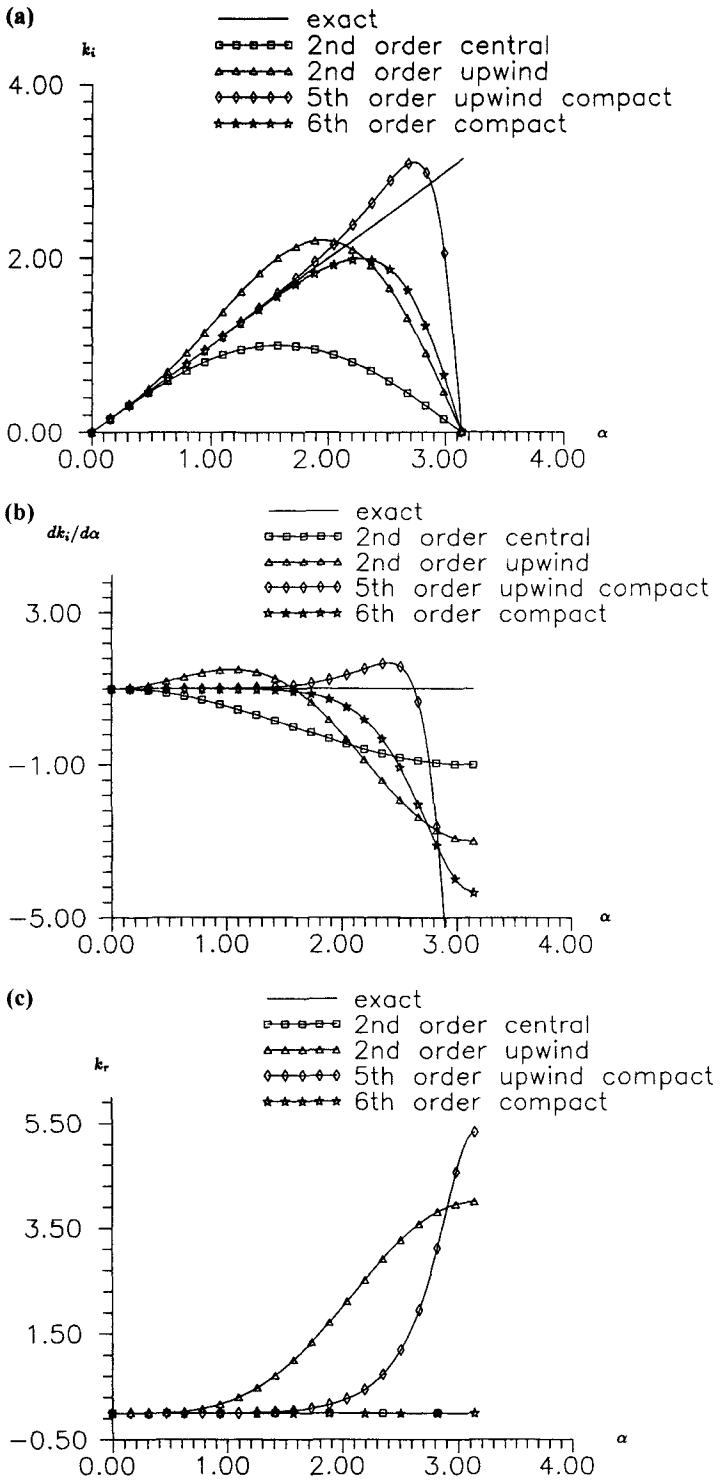

Figure 1. Variation of k_i (**a**), $\mathrm{d}k_i/\mathrm{d}\alpha$ (**b**), and k_r (**c**) vs. $k\Delta x$.

$$\mu_2 = \left[\sum C_{2m}\Delta x^{2m-1}\frac{\partial^{2m-1}f}{\partial x^{2m-1}}\right]\cdot f_u \Big/ \frac{\partial f}{\partial x}, \tag{6b}$$

$$a = \left[\sum C_{2m+1}\Delta x^{2m}\frac{\partial^{2m}f}{\partial x^{2m}}\right] \Big/ \frac{\partial^2 u}{\partial x^2}. \tag{6c}$$

They are more convenient for analysing the characteristics of numerical solution in the physical space. The coefficient μ' is related to approximation of the viscous term. Only the symmetrical approximation is used for the viscous term. The coefficient μ_2 obtained from the truncation error with even derivatives is related to the dissipativity. The stability requires nonnegativity of the coefficient μ_2. a is related to modification of the phase speed or the group velocity of wave packets for approximation of the convection term.

Equation (5) is useful for analyzing the behaviour of numerical solution and reconstructing the schemes for improvement of resolution of schemes. In the linear case for single Fourier component we have

$$\mu' = \left(\frac{K_d}{\alpha^2} - 1\right), \tag{7a}$$

$$\mu_2 = \frac{cK_r}{\alpha k}, \tag{7b}$$

$$a = \frac{c}{k}\left(\frac{K_i}{\alpha} - 1\right). \tag{7c}$$

2.2 *Dispersion effect*

For correct simulation of unsteady flow field with a range of scales, the dispersion effect in numerical solutions from approximation of the convection term must be considered.

2.2a *Classification of schemes by group velocity of wave packets:* The commonly used method of classification of schemes is by dissipativity of numerical solutions. The scheme is called dissipative if cK_r in (4) or μ_2 in (5) is positive. In the opposite case the scheme is unstable. The stable scheme is nondissipative if $K_r \equiv \mu_2 \equiv 0$.

The wave packets in numerical solutions are propagated by group velocity which defines the dispersion effect of schemes. It may greatly affect the numerical accuracy. In order to analyse the dispersion effect, schemes are classified by the group velocity of wave packets in numerical solutions. The group velocity in numerical solutions is defined as

$$D(\alpha) = \frac{\mathrm{d}cK_i}{\mathrm{d}\alpha} = cD^\circ(\alpha), \quad D^\circ(\alpha) = \frac{\mathrm{d}K_i}{\mathrm{d}\alpha}, \tag{8}$$

where $D^\circ(\alpha)$ is called density of group velocity.

By group velocity of wave packets the schemes are divided into three classes. The scheme is called faster (FST) if $D^\circ(\alpha) \geq 1$ for $0 \leq \alpha \leq \pi$. This means that numerical wave packets are propagated faster than physical ones. The scheme is called slower (SLW) if $D^\circ(\alpha) \leq 1$, in this case the numerical wave packets are propagated slower than physical ones; it is called mixed (MXD) if $D^\circ(\alpha) > 1$ for $0 < \alpha < \alpha_0 < \pi$ and $D^\circ(\alpha) < 1$ for $\alpha_0 < \alpha \leq \pi$.

The symmetrical schemes and weakly upwind biased schemes belong to SLW. Moderately and strongly upwind biased schemes are MXD, but strongly upwind biased schemes may be unstable ($cK_r < 0$). The second-order Pade scheme belongs to FST.

2.2b *Behaviour analysis of dispersion error:* It is obvious that the phase speed or the group velocity of wave packets with low wave numbers in numerical solutions are very close to the physical value. In the present paper this group velocity is called reference group velocity. The reference density of group velocity $D^\circ(\alpha) = 1$. Nonlinear dependence of K_i on $\alpha = k\Delta x$ leads to nonuniform group velocity for higher wave numbers. So different propagation direction of wave packets can be obtained in numerical solutions for higher wave numbers.

Consider a numerical example with the model equation

$$\frac{\partial u}{\partial t} + \frac{\partial u}{\partial x} = 0 \tag{9}$$

and initial condition

$$u(x, 0) = \exp(-16x^2)\sin(\alpha_0 x) + \{\exp[-16(x + 1.5)^2] + \exp[-16(x - 1.5)^2]\}\sin(\alpha_1 x). \tag{10}$$

The following five schemes are used:

(1) *Pade Scheme (FST)* *

$$F_j + F_{j-1} = 2(u_j - u_{j-1}). \tag{11a}$$

(2) *Second order central scheme (SLW)*

$$F_j = \delta_x^0 u_j. \tag{11b}$$

(3) *Second order upwind scheme (MXD)*

$$F_j = \delta_x^- [3u_j - u_{j-1}]/2. \tag{11c}$$

(4) *Second order central scheme with wide stencil (SLW)*

$$F_j = (u_{j+2} - u_{j-2})/4. \tag{11d}$$

(5) *Fifth order upwind compact scheme (MXD)*

$$\tfrac{3}{5}F_j^\pm + \tfrac{2}{5}F_{j\mp1}^\pm = \tfrac{1}{60}\delta_x^\mp(-f_{j\pm2}^\pm + 11f_{j\pm1}^\pm + 47f_j^\pm + 3f_{j\mp1}^\pm), \tag{11e}$$

where $\delta_x^\pm g_j = \mp(g_j - g_{j\pm1})$, $\delta_x^0 = (\delta_x^+ + \delta_x^-)/2$ and $\delta_x^2 = \delta_x^+\delta_x^-$.

*FST, SLW and MXD stand for "faster", "slower" and "mixed" – see § 2.2a for further details

Some results of (9) with initial condition (10) for $\alpha_0 = 100, \alpha_1 = 25$ are shown in figure 2a. It can be seen that all waves move toward the right. Scheme (3) has high dissipativity for high wave numbers. Low group velocity for scheme (4) is obvious for high wave numbers. Figure 2b shows the results for $\alpha_0 = 157, \alpha_1 = 25$. For this case the waves with high frequency for scheme (4) are standing waves. In figure 2c the results for $\alpha_0 = 194, \alpha_1 = 25$ are given. This figure shows that the group velocity for scheme (4) is negative.

From the above analysis the following conclusions can be obtained: For FST schemes all waves are moving in the same direction as the reference waves, but the high frequency waves are in front of the reference waves; for SLW schemes all waves are behind the reference waves. Some of them are moving in the same direction as the reference waves, some are standing waves, and some are moving in the opposite direction. For MXD schemes in numerical solutions, the Fourier components have all the possible motions of both FST and SLW schemes.

2.2c *Anisotropic effect:* In multi-dimensional problems the dispersion effect appears in the form of anisotropy. In order to analyse the anisotropic effect consider the following model equation

$$\frac{\partial u}{\partial t} + a\frac{\partial u}{\partial x} + b\frac{\partial u}{\partial y} = 0, \quad a, b = \text{const.}, \tag{12a}$$

with initial condition

$$u(x, 0) = \exp\{i[\mathbf{K} \cdot \mathbf{X}]\} \tag{12b}$$

where $\mathbf{K} = [k_1, k_2]^T, \mathbf{X} = [x, y]^T$, and k_1, k_2 are wave numbers in x and y directions respectively. Defining

$$\mathbf{l} = \left[\frac{a}{(a^2 + b^2)^{1/2}}, \frac{b}{(a^2 + b^2)^{1/2}}\right]^T,$$

it can be rewritten as

$$\mathbf{l} = [\cos\theta, \sin\theta]^T,$$

where θ is azimuthal angle.

The exact solution for (12a) with initial condition (12b) can be expressed as follows

$$u(\mathbf{X}, t) = \exp\{i[\mathbf{K} \cdot \mathbf{X} - (a^2 + b^2)^{1/2}\mathbf{K} \cdot \mathbf{l}t]\}. \tag{13}$$

The semi-discrete approximation for (12a)

$$\frac{\partial u}{\partial t} + a\frac{F_i}{\Delta x} + b\frac{F_j}{\Delta y} = 0, \tag{14a}$$

with initial condition

$$u(\mathbf{X}, 0) = \exp[i(\mathbf{K} \cdot \mathbf{X})], \tag{14b}$$

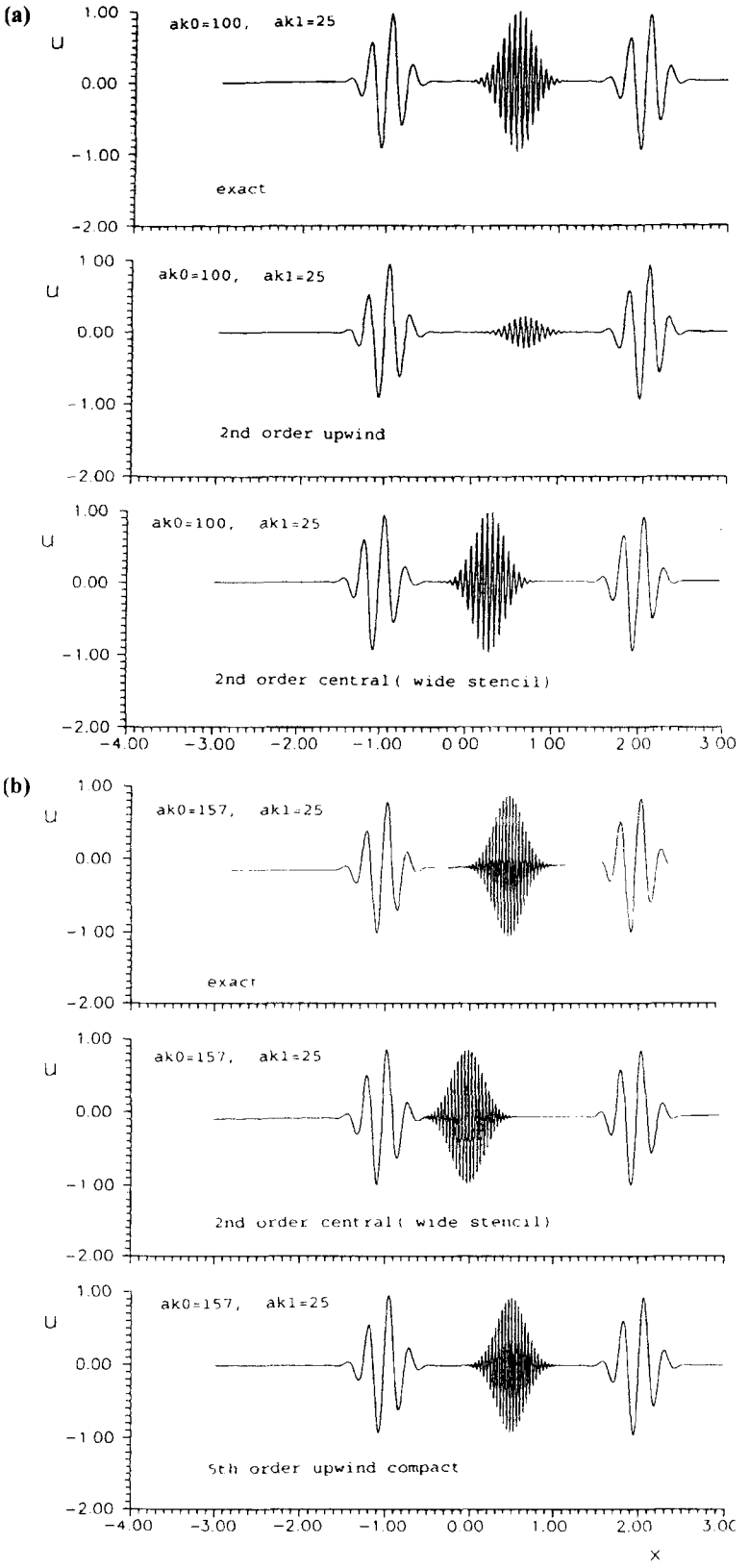

Figure 2.(a & b) (Caption on next page.)

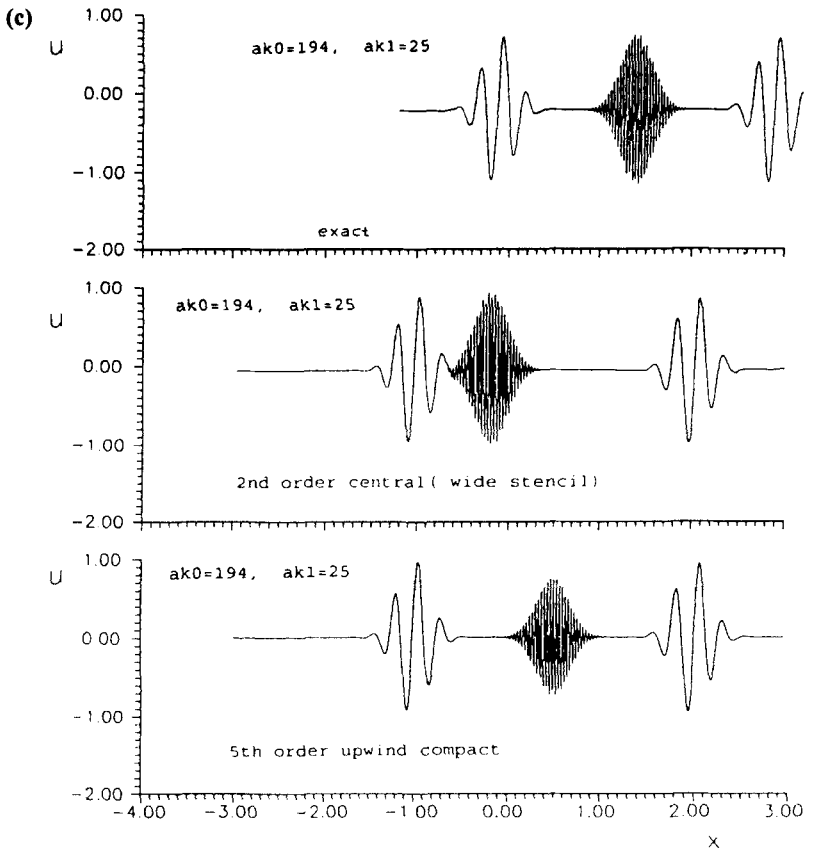

Figure 2. Numerical results for (10): (**a**) $\alpha_0 = 100, \alpha_1 = 25$; (**b**) $\alpha_0 = 157, \alpha_1 = 25$; (**c**) $\alpha_0 = 194, \alpha_1 = 25$.

has exact solution as follows

$$u(\mathbf{X}, t) = \exp\{-(a^2 + b^2)^{1/2}\mathbf{K} \cdot \mathbf{I}'_r t\} \cdot \exp\{i\mathbf{K} \cdot [\mathbf{X} - (a^2 + b^2)^{1/2}\mathbf{I}'_i t]\}, \quad (15)$$

$$\mathbf{I}'_r = \left[\cos\theta \frac{K_r^{(1)}}{\alpha}, \sin\theta \frac{K_r^{(2)}}{\beta}\right]^T, \quad \alpha = k_1 \Delta x,$$

$$\mathbf{I}'_i = \left[\cos\theta \frac{K_i^{(1)}}{\alpha}, \sin\theta \frac{K_i^{(2)}}{\beta}\right]^T, \quad \beta = k_2 \Delta y,$$

where $K_r^{(1)}$, $K_i^{(1)}$, vectors $\mathbf{I}'_r$ and $\mathbf{I}'_i$ are functions of α and β. For different schemes $\mathbf{I}'_r$ and $\mathbf{I}'_i$ are different. Consider the projection of numerical vectors $\mathbf{I}'_r$ and $\mathbf{I}'_i$ on the exact $\mathbf{I}$. For nondissipative schemes $\mathbf{I}_r \equiv 0$. In this case we have

$$\mathbf{I} \cdot \mathbf{I}' = (1/\omega)[\cos\theta K_i^{(1)} + \sin\theta K_i^{(2)}], \quad 0 \le \theta \le 2\pi, \quad (16)$$

where $K_i^{(1)} = K_i^{(1)}(\alpha)$, $K_i^{(2)} = K_i^2(\beta)$, $\alpha = \omega\cos(\theta)$, $\beta = \omega\sin(\theta)$ and $\omega = (\alpha^2 + \beta^2)^{1/2}$.

The five approximations in (11) and the sixth order symmetric compact approximation are used for discretizing the space derivative in (12a), the three-step R–K method is used

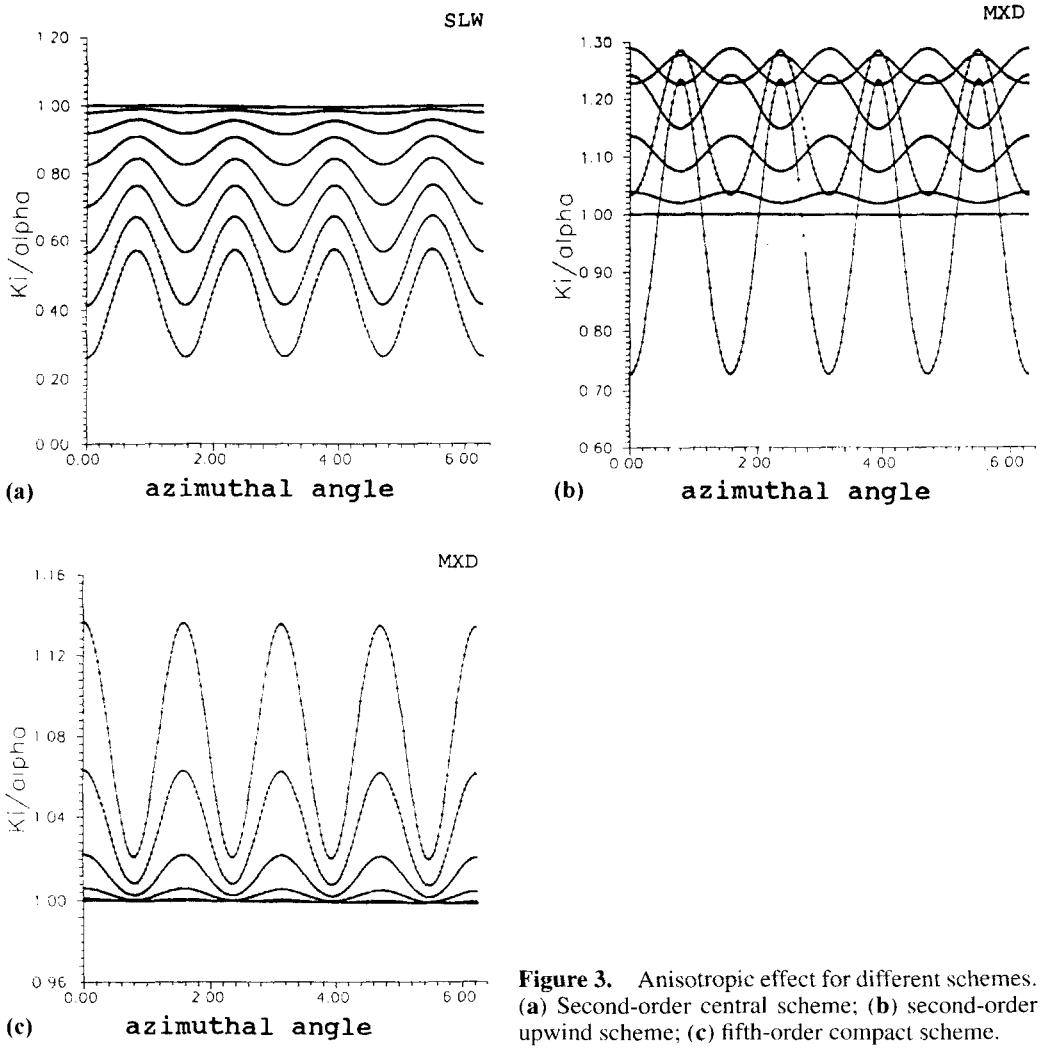

Figure 3. Anisotropic effect for different schemes. (**a**) Second-order central scheme; (**b**) second-order upwind scheme; (**c**) fifth-order compact scheme.

for approximation of the time derivative for SLW and MXD schemes, and for the FST scheme in (11) the Crank–Nicolson method is used. The computed results from (16) with $\omega_m = m\pi/10, m = 0, 1, \ldots, 9, 0 \leq \theta \leq 2\pi$ for different schemes are shown in figure 3. From these results it can be seen that different schemes have different anisotropic effects for high wave numbers. On increasing the order of accuracy of approximation, the range of wave numbers with small anisotropic effect can be enlarged.

3. Improvement of numerical solutions

Only a one-dimensional case is considered in this section. Three methods of improvement of numerical solutions are presented.

3.1 *Increasing the order of accuracy of approximation*

From the figures of K_i, K_r vs. α (figure 4) it can be seen that approximation error of schemes becomes smaller with increasing the order of accuracy in a wide range of wave numbers. For the symmetric difference schemes $K_r = 0$. For fifth order upwind compact finite difference scheme (UCFD5), K_r is small in a wider range of wave numbers and it is large for super high wave numbers. It is useful to damp the aliasing error when the nonlinear problems are solved.

It is obvious that the stencil size is enlarged with increase in the order of accuracy. This leads to difficult treatment of the boundary conditions, and difference approximations at the points next to the boundary have to be treated specially. It must be noted that the strongly one-side biased schemes at boundary points and near boundary points may not be stable. In order to get high-order accurate scheme with less stencil size, the super compact finite difference scheme (SCFDM) developed by us (Ma Yanwen & Fu Dexun 1996) is introduced here briefly.

The basic idea for construction of the traditional difference schemes is that the approximation of the derivatives is expressed explicitly by a linear combination of the function values at the points near the considered point. For the compact scheme we have a linear combination of both the function values and their derivatives at grid points. For obtaining the approximation of derivative a linear system has to be solved. For the SCFDM we use a linear combination of the function values themselves, the derivatives and their higher derivatives at the grid points. For example, consider discretization of $\partial u/\partial x$ with symmetric approximation.

The traditional difference approximation can be expressed as

$$F_j = \sum_l b_l \frac{u_{j+l} - u_{j-l}}{2l}. \tag{17}$$

For compact difference approximation we have

$$\sum_l \frac{a_l}{2}(F_{j+l} + F_{j-l}) = \sum_l \frac{b_l}{l}\frac{u_{j+l} - u_{j-l}}{2}, \tag{18}$$

$$\sum a_l = \sum b_l = 1.$$

SCFDM considers approximations of all necessary derivatives as unknown. SCFDM for odd derivatives with uniform grid mesh can be written as

$$-\tfrac{1}{2}LF_{j-1} + (L + A)F_j - \tfrac{1}{2}LF_{j+1} = \delta_x^0 f_j e \tag{19}$$

where L, A are $M \times M$ matrices, F and e are M dimensional vectors, $f_j^{(2k-1)}/\Delta x^{2k-1}$ is an approximation for $(2k-1)$th derivative $\partial^{2k-1} f/\partial x^{2k-1}$ with the accuracy of order $2(M - K + 1)$, and

$$A = \begin{bmatrix} 1/1!, 1/3!, 1/5!, \ldots 1/(2M-1)! \\ 0, 1/2!, 1/4!, \ldots, 1/[2(M-1)]! \\ 0, 0, 1/2!, \ldots, 1/[2(M-2)]! \\ \ldots\ldots\ldots\ldots\ldots\ldots\ldots\ldots \\ 0, 0, 0, \ldots, 1/2! \end{bmatrix}$$

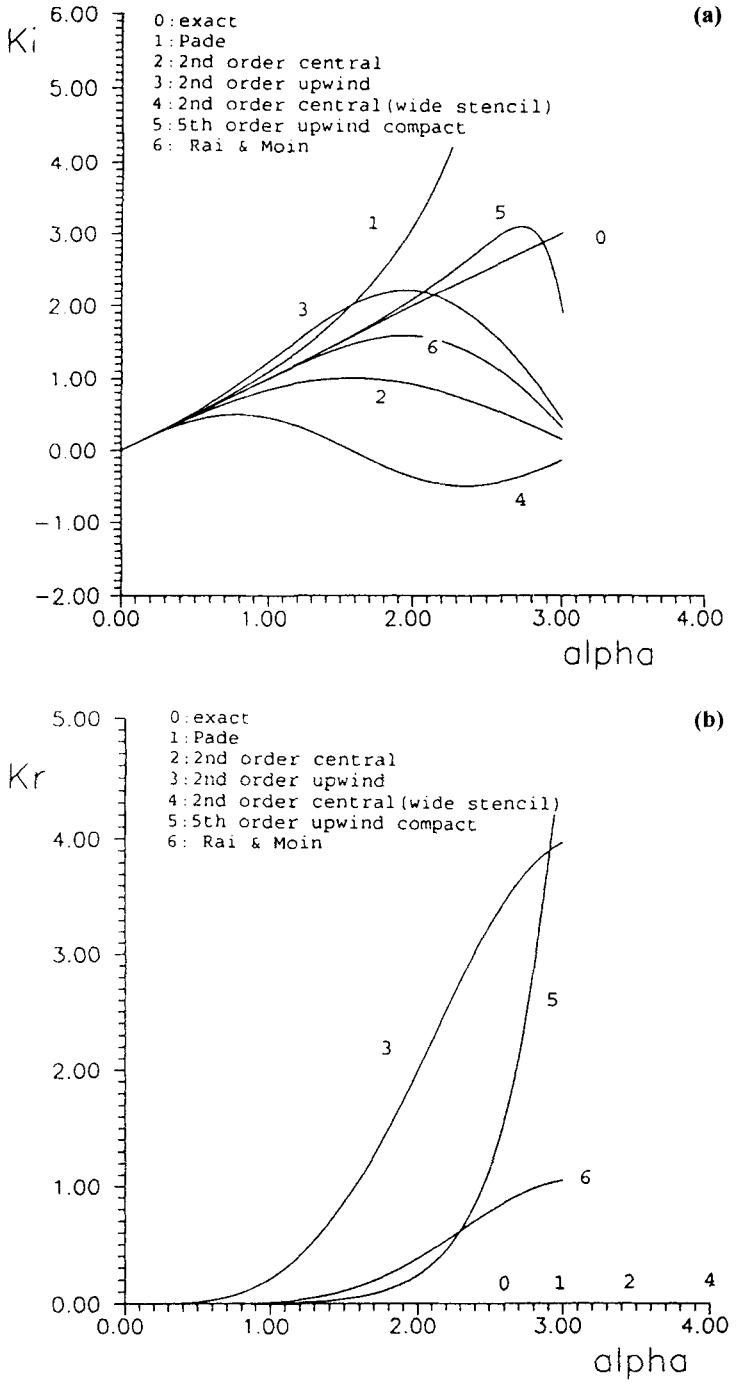

Figure 4. Variation of k_i (**a**) and k_r (**b**) vs. α.

$$L=\begin{bmatrix} 0 & 0 & 0\cdots 0 & 0 \\ 1 & 0 & 0\cdots 0 & 0 \\ 0 & 1 & 0\cdots 0 & 0 \\ \cdots & \cdots & \cdots & \cdots \\ 0 & 0 & 0\cdots 0 & 0 \\ 0 & 0 & 0\cdots 1 & 0 \end{bmatrix}$$

$$F=[f^{\langle 1\rangle}, f^{\langle 2\rangle}, \ldots, f^{\langle 2M-1\rangle}]^T.$$

For the case $M = 1$ we have the traditional central difference approximation

$$f_j^{\langle 1\rangle} = \delta_x^0 f_j. \tag{20}$$

For the case $M = 2$ from (19) we can get the classical fourth order accurate compact difference approximation

$$(1/6)f_{j-1}^{\langle 1\rangle} + (2/3)f_j^{\langle 1\rangle} + (1/6)f_{j+1}^{\langle 1\rangle} = \delta_x^0 f_j. \tag{21}$$

For the case $M = 3$ from (19) we can get three equations for $f^{\langle 1\rangle}$, $f^{\langle 2\rangle}$ and $f^{\langle 3\rangle}$. It can be shown that the same order of accuracy of approximation SCFDM has higher resolving efficiency.

3.2 *Method of group velocity control (GVC)*

As mentioned earlier, the dispersion effect of schemes leads to production of oscillation in numerical solution. If FST schemes are used to compute the shocks, the high frequency waves appear in front of the reference waves, and if SLW schemes are used, the high frequency waves appear behind the reference waves. In order to improve numerical solutions the method of group velocity control can be used. This can be done by using the function

$$SS(u) = sign\left(\frac{\partial u}{\partial x}\cdot\frac{\partial^2 u}{\partial x^2}\right). \tag{22}$$

Suppose we have a given difference approximation (2). The scheme used can be reconstructed so that it is FST behind the reference waves where $SS(u) > 0$, and is SLW in front of the reference waves where $SS(u) < 0$. According to the modified equation (5), consider the following equation

$$\frac{\partial u}{\partial t}+\frac{\partial f}{\partial x}=\frac{\partial}{\partial x}\left(\mu\frac{\partial u}{\partial x}\right)+\sigma_0\frac{\partial}{\partial x}\left[SS(u)\cdot sign(a)\cdot a\frac{\partial^2 u}{\partial x^2}\right], \tag{23}$$

where

$$a=\left[\sum C_{2m+1}\Delta x^{2m}\frac{\partial^{2m} f}{\partial x^{2m}}\right]\Big/\frac{\partial^2 u}{\partial x^2}. \tag{24}$$

In application only the leading term is used in (24). With the same way as for discretizing the original equation (1) we can get a newly reconstructed scheme from (23). With suitable

choice $\sigma_0 (0 < \sigma_0 < 1)$ the resolution of reconstructed scheme will be improved. This method can be used to reconstruct 2-D and 3-D schemes easily. When flow field structures with small scales and shocks are of interest, higher-order accurate schemes need to be reconstructed.

3.3 *Method of accuracy balance for components with different wave numbers*

The main purpose of the improvement of numerical methods is to get high resolution efficiency over a wider range of wave numbers on the given mesh, and not only formal accuracy. It can be seen that the main contribution of increasing the order of accuracy of approximation is to the Fourier components with low wave numbers. The components with high or super high wave numbers are not so sensitive to increasing the formal order of accuracy of approximation. The basic idea for the method of accuracy balance is to use wider stencil size to get high resolution for components with higher wave numbers.

Consider the fourth order compact difference approximation. In order to get high resolving efficiency over a wider range of wave numbers, this scheme can be reconstructed as follows

$$\sum_{l=-1}^{1} \beta_l \left[\frac{1}{6} F_{j+1+l} + \frac{2}{3} F_{j+l} + \frac{1}{6} F_{j-1+l} - \delta_x^0 u_{j+l} \right]$$

$$= \sum_{l=-1}^{1} r_l \left[\frac{1}{2} (u_{j+l+2} - u_{j+l-2}) - (u_{j+l+1} - u_{j+l-1}) - \delta_x^2 F_{j+l} \right]. \tag{25}$$

It is obvious that the leading term of truncation error of this equation is $O(\Delta x^5)$. Only consider the symmetrical approximation. Symmetry requires $\beta_1 = \beta_{-1}, r_1 = r_{-1}$. Suppose $\beta_0 = 1$. Putting the Fourier component into (25) we can get

$$K_i = \frac{3 \sin\alpha [1 + 2\beta_1 \cos\alpha] + 3[\sin 2\alpha - 2\sin\alpha][r_0 + 2r_1 \cos\alpha]}{(1 + 2\beta_1 \cos\alpha)(\cos\alpha + 2) + 6(\cos\alpha - 1)(r_0 + 2r_1 \cos\alpha)}, \tag{26}$$

$$K_r = 0.$$

The coefficient r_0, r_1 and β_1 in (26) can be defined from the requirement $K_i(\alpha_i) = \alpha_i$, $i = 1, 2, 3$. In figure 5 the modified K_i is shown. It can be seen that the range of wave numbers with high resolving efficiency for modified scheme is much improved.

3.4 *Numerical examples*

Consider the model equation

$$\frac{\partial u}{\partial t} + \frac{\partial u}{\partial x} = 0. \tag{27}$$

Example 1. Semi-circular wave: The initial condition is defined as

$$u(x, 0) = \begin{cases} 0, & x \leq -0.5, \\ (0.25 - x^2)^{1/2}, & -0.5 < x < 0.5, \\ 0, & 0.5 < x. \end{cases}$$

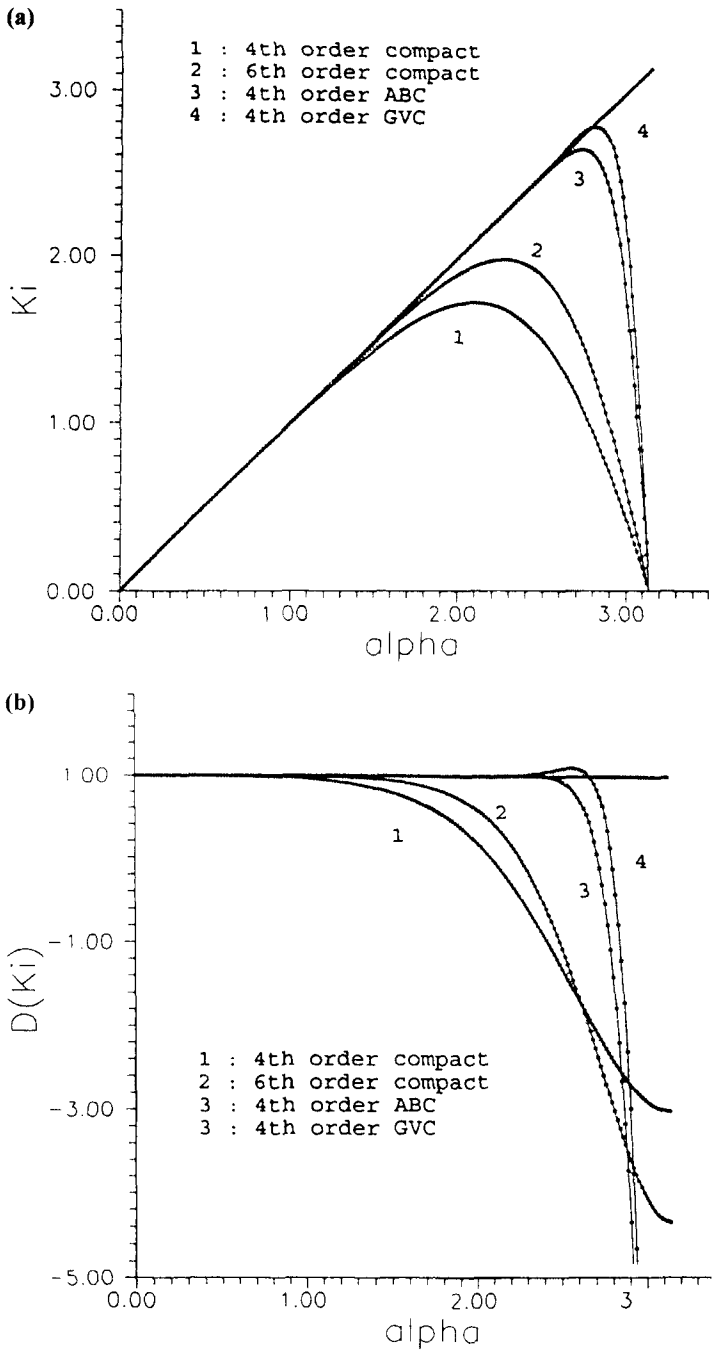

Figure 5. Variation of k_i (**a**), $D(k_i)$ (**b**) vs. α.

Example 2. Square wave: The initial condition is given as

$$u(x,0) = \begin{cases} 0, & x \le -0.5, \\ 1, & -0.5 < x < 0.5, \\ 0, & 0.5 < x. \end{cases}$$

Different schemes are used to solve (27). Some results are given in figure 6. From the computed results it can be seen that the resolution of numerical solutions is much improved with group velocity control, and high order accurate schemes are needed for correct simulation of complex flow field with small structures. The numerical practice shows that the method of accuracy balance is not so effective.

4. Numerical simulation of compressible mixing layer

High-order accurate schemes with GVC has been used to solve the full time-dependent 3-D compressible N–S equations. Basic idea of numerical method is as follows: the fifth order accurate compact upwind finite difference (UCFD5) relation (Fu Dexun & Ma Yanwen 1995) is used to approximate the convection term in the N–S equations, the sixth order accurate symmetrical compact difference relation (Lele 1992) is used to approximate the viscous term, and a third order R–K method is used to approximate the time derivatives. Periodic boundary conditions are used in the streamwise and spanwise directions. In the y direction non-reflecting boundary conditions are used.

The effect of initial disturbance on coherent structures in the compressible mixing layer with convection Mach number $M_c = 0.8$ is studied. The convection Mach number is defined as $M_c = (U_1 - U_2)/(C_1 + C_2)$, where U_1 and U_2 are the free-stream velocities, C_1 and C_2 are the corresponding sound speeds. In the computation, $U_2 = -U_1$ is taken. The mean streamwise velocity and the passive scalar field are specified by hyperbolic-tangent profile. The mixture fraction of passive scalar function has value $+1$ in the field with velocity U_1 and -1 in the field with U_2. The Reynolds number is based on the vorticity thickness and the velocity difference between the two streams. The vorticity thickness is defined as $\delta_w = (U_1 - U_2)/|\mathrm{d}u/\mathrm{d}y|_{\max}$.

Two cases of initial perturbations are taken in computations.

(A) *1st case:* A pair of equal and opposite oblique instability waves is taken as initial perturbation in computation

$$\begin{aligned} f' &= \alpha_1 \mathrm{Re}\{\hat{f}(\alpha,0)e^{i\alpha x}\} \\ &\quad + \alpha_2 \mathrm{Re}\{\hat{f}(\alpha,\beta)e^{i(\alpha x+\beta z)} + \hat{f}(\alpha,-\beta)e^{i(\alpha x-\beta z)}\}, \\ f' &= u', v', w', p', T', \\ \alpha_1 &= 0, 0.05, \alpha_2 = 0.025, \end{aligned} \tag{28}$$

where u, v and w are components of the velocity vector in the x, y and z direction respectively, T is temperature and p is pressure. The eigenfunctions $\hat{f}$ are obtained from solving the linearized N–S equations (Wang Qiang *et al* 1997).

(B) *2nd case:*

The 2-D linear instability waves plus probability function in the Z direction are taken as the initial perturbation in order to get vorticity pairing. The initial perturbation for

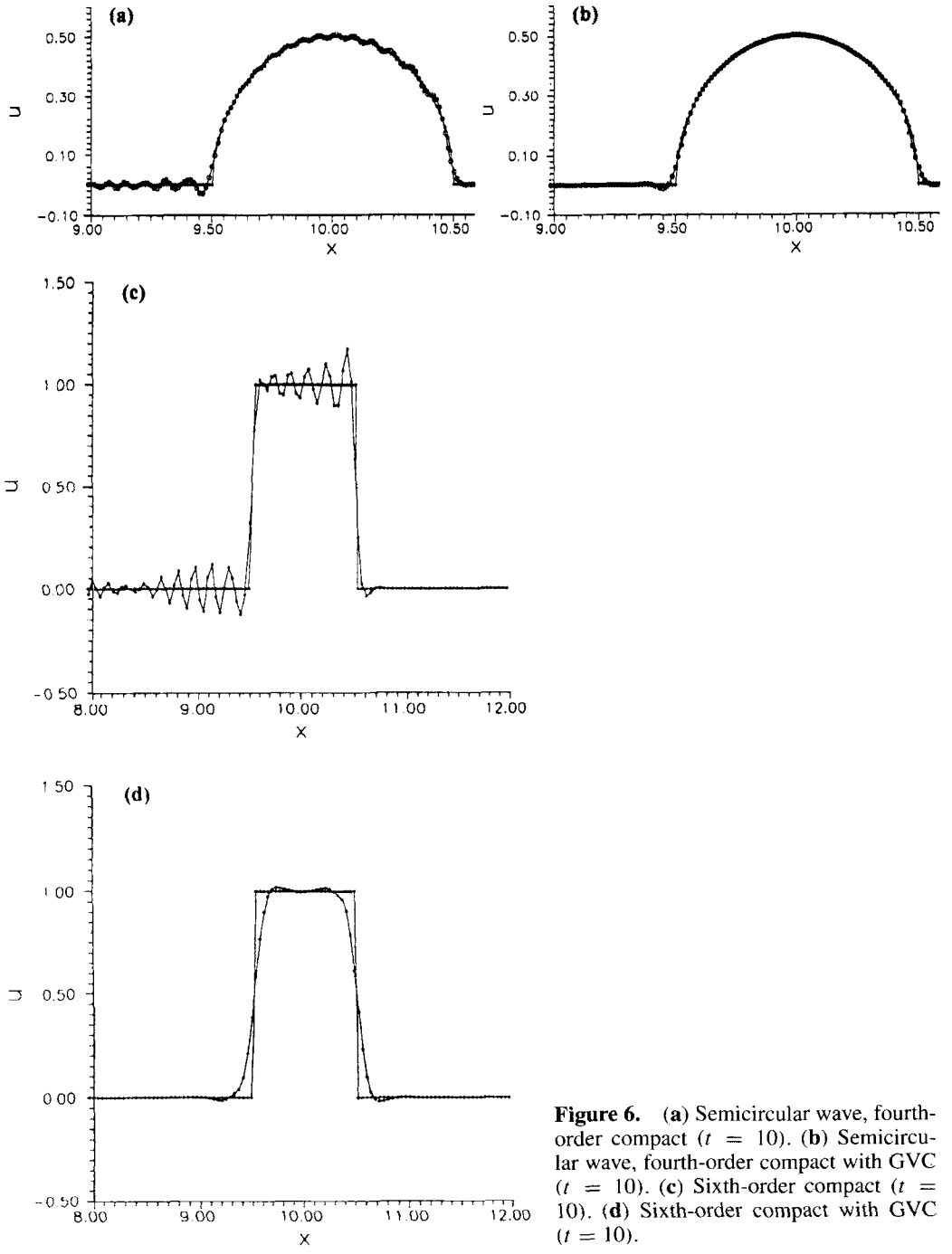

Figure 6. (**a**) Semicircular wave, fourth-order compact ($t = 10$). (**b**) Semicircular wave, fourth-order compact with GVC ($t = 10$). (**c**) Sixth-order compact ($t = 10$). (**d**) Sixth-order compact with GVC ($t = 10$).

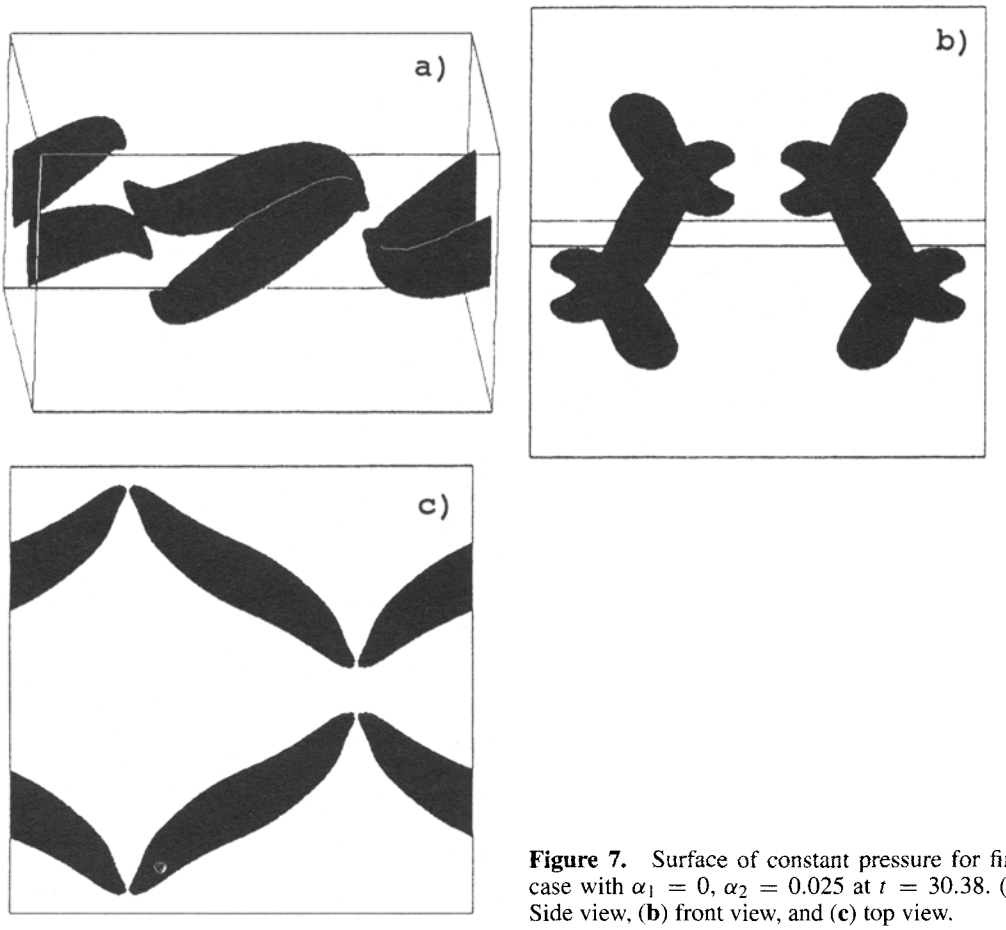

Figure 7. Surface of constant pressure for first case with $\alpha_1 = 0$, $\alpha_2 = 0.025$ at $t = 30.38$. (**a**) Side view, (**b**) front view, and (**c**) top view.

velocity is

$$
\begin{aligned}
u' &= \varepsilon_1[\varphi'_{1r}\cos(\alpha_1 x) - \varphi'_{1i}\sin(\alpha_1 x)] \\
&\quad + \varepsilon_2[\varphi'_{2r}\cos(\alpha_2 x) - \varphi'_{2i}\sin(\alpha_2 x)], \\
v' &= \varepsilon_1[\varphi_{1r}\sin(\alpha_1 x) + \varphi_{1i}\cos(\alpha_1 x)]\alpha_1 \\
&\quad + \varepsilon_2[\varphi_{2r}\sin(\alpha_2 x) + \varphi_{2i}\cos(\alpha_2 x)]\alpha_2 - (K_z/2)e^{-y^2}\cos(K_z z), \\
w' &= -\varepsilon_z e^{-y^2}\sin(K_z z)\cdot y, \\
\varepsilon_1 &= \varepsilon_2 = 0.05, \\
\alpha_1 &= 0.4446,\ \alpha_2 = \tfrac{1}{2}\alpha_1.
\end{aligned}
\tag{29}
$$

The eigenfunctions φ_{1r}, φ_{1i}, φ_{2r}, φ_{2i} are obtained from linear stability theory.

Some numerical results for the first case with Re = 560 and $\alpha_1 = 0$ at $t = 30.38$ are given in figures 7–9. In figure 7 a surface of constant pressure of small value is shown and we can see that symmetrical $\wedge$ vortex structure according to x–y plane is formed from the initial two equal and opposite oblique instability waves. It is similar to the $\wedge$-structures in transitional boundary layer flow. In figure 8 the contours of mixture fraction field are

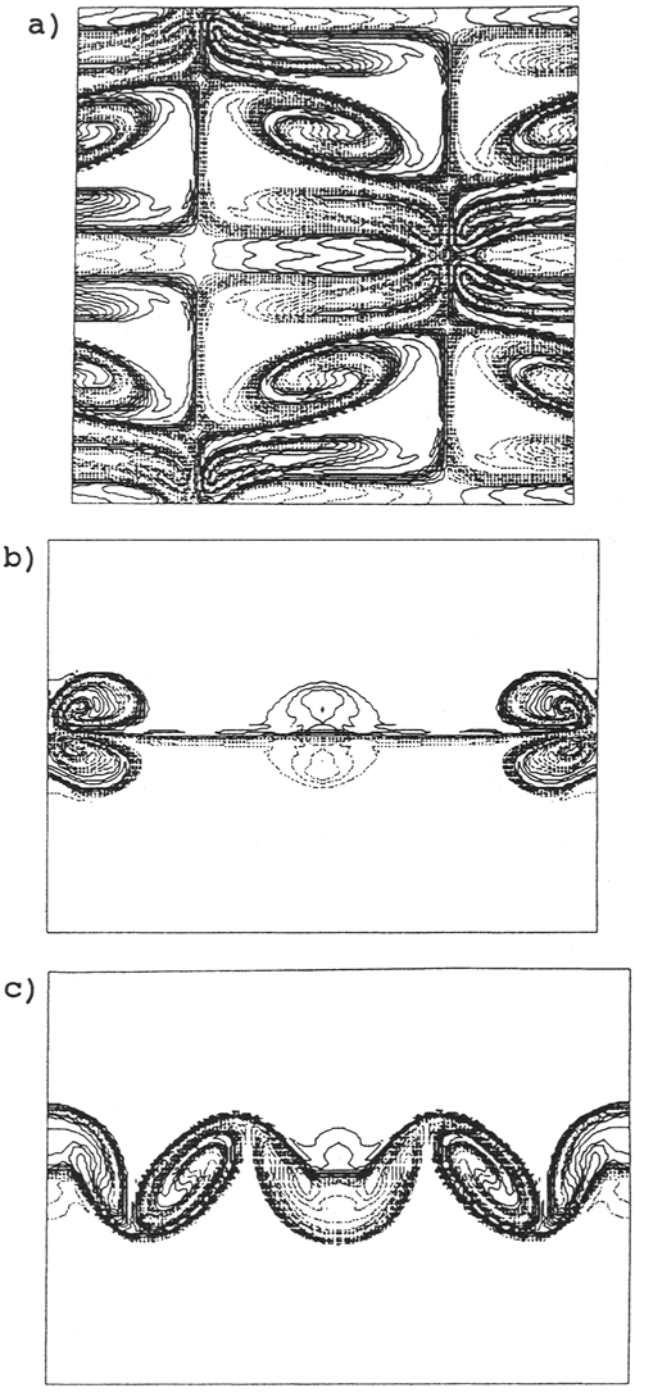

Figure 8. Contours of mixture fraction field for first case with $\alpha_1 = 0$, $\alpha_2 = 0.025$ at $t = 30.38$. (**a**) (x, z) plane at $y = 0$, (**b**) (y, z) plane at $z = (1/4)Lx$, (**c**) (y, z) plane at $x = (1/2)Lx$.

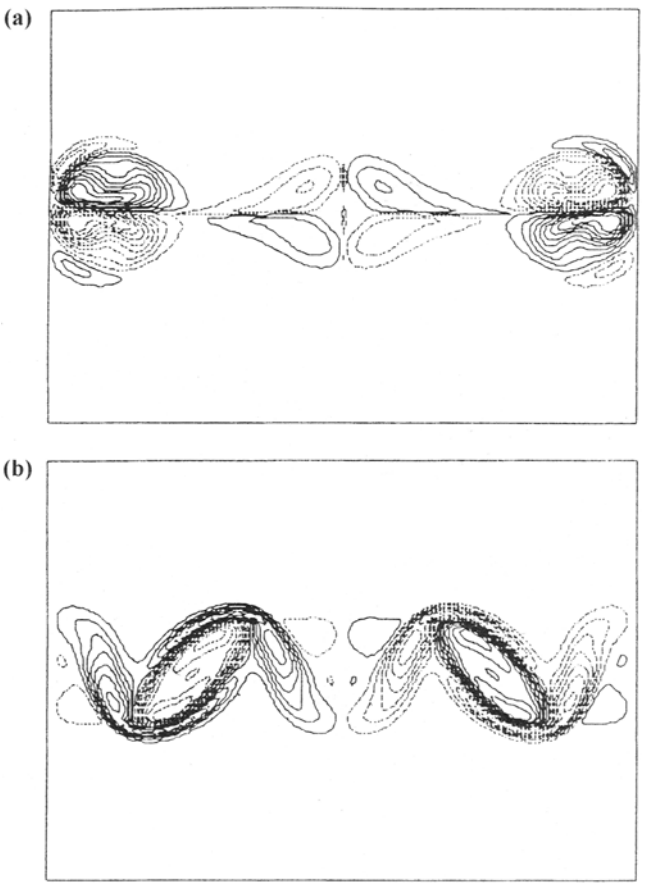

Figure 9. Contours of streamwise vorticity for the first case with $\alpha_1 = 0$, $\alpha_2 = 0.025$, solid lines: positive values, dashed lines: negative values. (**a**) (y, z) plane at $x = (1/4)Lx$, (**b**) (y, z) plane at $x = (1/2)Lx$.

given. Figure 8a shows a structure in the x–z plane at $y = 0$. Four main rotational regions with three-dimensional saddle points are obvious.

The mushroom shaped structures in the y–z plane at $x = Lx/4$ and $Lx/2$ are shown in figures 8b and 8c respectively. The contours of streamwise vorticity for the first case, with $\alpha_1 = 0, \alpha_2 = 0.025$, are given in figure 9 where solid lines correspond to positive values, and dashed lines correspond to negative values. We can see that the positive spanwise vorticity appears in the field at the beginning of the flow transition and an oblique rib structure is formed for streamwise vorticity.

The surface of constant pressure of small value for the first case with $\mathrm{Re} = 400$, $\alpha_1 = 0.05, \alpha_2 = 0.025$ at $t = 30.2$ is shown in figure 10. The $\wedge$ vortex structure is also formed. But it is not symmetrical to the x–y plane. That is the effect of initial two-dimensional instability wave on the structures. In the development of flows in numerical simulation for the first case there are no pairing or shocks formed.

All the above structures are very like the structures obtained by Sandham & Reynolds (1991) with the mixed spectral and high-order finite difference method. It can be seen that

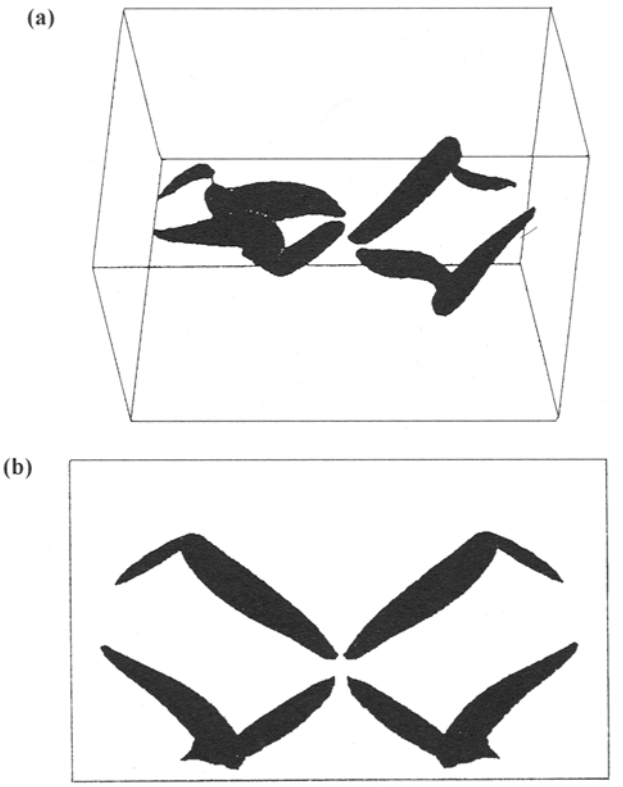

Figure 10. (**a**) Pressure contour for the second case at $t = 30.2$. (**b**) Surface of constant pressure for first case with $\alpha_1 = 0.05$, $\alpha_2 = 0.025$ at $t = 30.2$. (**a**) Side view, (**b**) top view.

the high-order difference method presented in this paper is efficient for simulating the 3-D complex flow field.

In figure 11 are shown some numerical results for the second case with Re $= 400$ and $M_c = 0.8$. Vortex pairing can be seen at time $t = 66$ (figure 11a). A shock wave is generated during the time of pairing as for the 2-D case. The shock wave leads to positive spanwise vorticity in the 3-D flow field. It is important for the formation of 3-D coherent structures (figure 11b) and flow transition.

5. Conclusion

Analysing the behaviour of numerical solutions is useful for correct simulation of complex flow fields with a range of scales. Understanding and controlling both of dissipativity and dispersion effects in numerical solutions are important for correctly capturing the small structures in complex flow fields. A high-order accurate finite difference method with group velocity control is suggested for reduction of numerical dissipativity and dispersion and it is used to simulate the compressible mixing layer.

Two kinds of initial conditions for simulating the compressible mixing layer are discussed. When equal and opposite waves are taken as the initial perturbation, for all variables

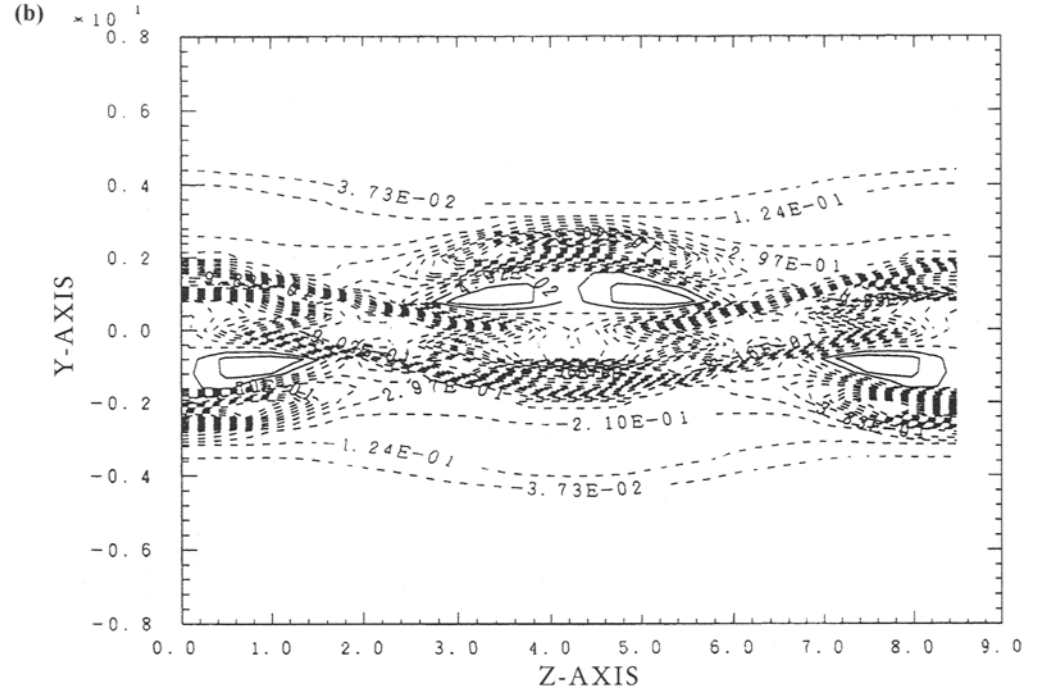

Figure 11. (**a**) Surface of constant spanwise vorticity for second case at time of pairing ($t = 66$). (**b**) Contours of spanwise vorticity for second case at $t = 93$; solid lines: positive values, dashed lines: negative values.

$\wedge$-vortex can be found and 2-D initial perturbation is larger (case 1, $\alpha_1 \neq 0$). When 2-D initial perturbation is added to all velocity components, but 3-D perturbation is added only to velocity components v and w, we can see rolling up, pairing and formation of shocks. Shock formation leads to production of positive spanwise vorticity. It is important for formation of 3-D coherent structures and flow transition.

The authors are grateful to the National Natural Science Foundation of China for financial support.

References

Fu Dexun, Ma Yanwen 1995 High resolution schemes. *Computational fluid dynamics review* (eds) M Hafez, K Oshima (New York: John Wiley & Sons) pp 234–250

Fu Dexun, Ma Yanwen 1997 A high order accurate difference scheme for complex flow fields. *J. Comput. Phys.* 134: 1–15

Lele S K 1992 Compact finite difference schemes with spectral-like resolution. *J. Comput. Phys.* 103: 16–42

Ma Yanwen, Fu Dexun 1996 Super compact finite difference method (SCFDM) with arbitrarily high accuracy. *Comput. Fluid Dynamics J.* 5: 259–276

Rai M M, Moin P 1991 Direct simulation of turbulent flow using finite-difference scheme. *J. Comput. Phys.* 96: 15–53

Sandham N D, Reynolds W C 1991 Three-dimensional simulation of large eddies in the compressible mixing layer. *J. Fluid Mech.* 224: 133–158

Trefethen L 1982 Group velocity in finite difference schemes. *SIAM Rev.* 24: 113–136

Wang Qiang, Fu Dexun, Ma Yanwen 1997 Numerical computation of stability for the compressible mixing layer. *Chinese J. Comput. Phys.* 14: 413–417 (in Chinese)